Ultramicroscopy 201 (2019) 38–48

Contents lists available at ScienceDirect

Ultramicroscopy

journal homepage: www.elsevier.com/locate/ultramic

Low-energy electron properties: Electron inelastic mean free path, energy loss function and the dielectric function. Recent measurements, applications, and the plasmon-coupling theory

C.T. Chantler*, J.D. Bourke

School of Physics, University of Melbourne, Parkville, Vic, 3010 Australia

ARTICLE INFO

Keywords:
Electron energy loss spectra
Inelastic mean free paths
Dielectric function
Electron spectroscopy

ABSTRACT

We review new self-consistent models of inelastic electron scattering in condensed matter systems for accurate calculations of low-energy electron inelastic mean free paths (IMFPs) for XAFS and low energy diffraction. The accuracy of theoretical determinations of the electron IMFP at low energies is one of the key limiting factors in current XAFS modeling and Monte Carlo transport. Recent breakthroughs in XAFS analysis show that there exist significant discrepancies between theoretical and experimental IMFP values, and that this can significantly impact upon extraction of other key structural parameters from both XANES and XAFS. Resolution of these discrepancies is required to validate experimental studies of material structures, and is particularly relevant to the characterization of small molecules and organometallic systems for which tabulated electron scattering data is often sparse or highly uncertain.

Novel models implement plasmon coupling mechanisms for the first time, in addition to causally-constrained lifetime broadening and high-precision density functional theory, and enables dramatic improvements in the agreement with recent high profile IMFP measurements. We discuss a theoretical approach for IMFP determination linking the optical dielectric function and energy loss spectrum of a material with its electron scattering properties and characteristic plasmon excitations. We review models inclusive of plasmon coupling, allowing us to move beyond the longstanding statistical approximation and explicitly demonstrate the effects of band structure on the detailed behaviour of bulk electron excitations in a solid or small molecule. This interrogates the optical response of the material, which we obtain using density functional theory. We find that new developments dramatically improve agreement with experimental electron scattering results in the low-energy region (30 eV → 200 eV) where plasmon excitations are dominant. Corresponding improvements are therefore made in Low Energy Electron Transport, LEEM, theoretical XAFS spectra and detector modelling.

1. Background for low energy electron properties

The origins of quantum oscillators and resonance scattering and losses is found in Drude and Einstein models extended to Debye and Drude-Sommerfeld models with Fermi-Dirac statistics for the electron by 1928 [1–4]. Much of the understanding of scattering, Compton scattering and inelastic scattering has also been based upon a free electron gas model [5,6]. Perhaps surprisingly, extensions of the Drude-Sommerfeld model into angle-dependent inelastic scattering and q-space extensions are still active and prevalent in 2018.

Major and dramatic advances were made [7,8] over the intervening decades, still based on a free electron gas model. Meanwhile of course the understanding of the solid state, regular arrays of atoms, conductors and dielectrics developed apace. In particular the idea of a plasmon as a plasma oscillation and propagation developed, with the observation of plasmons by energy losses in units of $\hbar\omega_p$ when electrons pass through thin metallic films [9].

Much of this core understanding is presented in classical texts [10–12]. As early as 1982, Levine and Louie attempted to modify the Drude-Sommerfeld basis away from the free electron gas model to account for the band gap in semiconductors [13].

The major breakthrough in the understanding and modelling of electron properties came with Penn in 1987 [14] which was then able to link up arbitrary solid state structure and behaviour from experimental or theoretical optical limit data to evaluate electron and plasmon inelastic scattering from band theory. In the same period there has been development of a plethora of density functional theories (DFTs), effective band theories and plasmon theories with many

* Corresponding author.
E-mail address: chantler@unimelb.edu.au (C.T. Chantler).

https://doi.org/10.1016/j.ultramic.2019.03.014
Received 20 December 2018; Accepted 21 March 2019
Available online 26 March 2019

contributions from many authors. More recently we have seen the discrepancies of inelastic mean free path theory at low energies [15–17] leading to the development and insight of coupled plasmon theory, a key topic of this paper and review [18,19].

The Drude-Sommerfeld model [4] permitted independent oscillators (electrons), as the implementation of Fermi-Dirac statistics of a free electron gas with a set i of eigenvalues of possible resonant energies of absorption ω_i with a degeneracy or number of oscillators N_i and an effective mass m with a damping term (lifetime) γ_i to yield the dielectric function or permittivity ε as a function of frequency ω, with the oscillators providing a shift from the permittivity in free space ε_0:

$$\varepsilon = \varepsilon_0 + \left(\frac{e^2}{m} \Sigma_i \frac{N_i}{(\omega_i^2 - \omega^2) - i\omega\gamma_i/m} \right) \tag{1}$$

While N_i was interpreted as the number of electrons, it is a simple matter to reinterpret this for plasmons as the fractional charge of a collective plasma (electron) wave. However, whereas the permittivity of a photon is well-represented by this functional, for an electron wave this is the 'optical limit' i.e. for forward scattering or with a change of wavevector $q = 0$. For elastic or inelastic scattering for the transport of a plasmon or electron wave, this functional needs to be extended into q-space. The simplest is the quadratic extension into q-space [20]:

$$\omega_q = \omega_i + \alpha \frac{\hbar q^2}{2m} \tag{2}$$

The other popular approach is the quartic extension into q-space:

$$\omega_q^2 = \omega_i^2 + \beta v_F^2 q^2 + \left(\frac{\hbar q^2}{2m} \right)^2 \tag{3}$$

Where $\beta = 1/3$ is recommended by some as the low-q limit of Thomas-Fermi theory [21–23], also used in major recent compilations [24,25]. Conversely, the coefficient $\beta = 3/5$ has been strongly proposed [26]. These limits, while popular in modern computations and tabulations, have particular limitations from causality, experimental data [15,16] and the nature of the Bethe Ridge [27]. The fundamental question, which we attempt to survey here, is what is the nature of the interaction of electrons with matter?

2. Inelastic mean free path (IMFP) theory - optical data models

The optical data model deals with the determination of the electron energy loss function (ELF), which is the principal determinant of the electron IMFP λ following

$$\lambda(E)^{-1} = \frac{\hbar}{a_o \pi E} \int_0^{\frac{E-E_F}{\hbar}} \int_{q_-}^{q_+} \frac{1}{q} \mathrm{Im}\left[\frac{-1}{\varepsilon(q,\omega)} \right] dq d\omega \tag{4}$$

The term $\mathrm{Im}\left[\frac{-1}{\varepsilon(q,\omega)}\right]$ is the electron ELF, and may be interpreted as a relative probability of an excitation of energy $\hbar\omega$ and momentum $\hbar q$ propagating in the medium [28]. The terms a_0 and m are the Bohr radius and electron mass, while the Fermi energy, E_F, is defined relative to the bottom of the conduction band. The limits of the momentum integral are given by

$$q \pm = \sqrt{\frac{2mE}{\hbar^2}} \pm \sqrt{\frac{2m}{\hbar^2}(E - \hbar\omega)} \tag{5}$$

Within this model the problem of calculating the electron IMFP, the mean distance between successive inelastic collisions measured along the electron's trajectory, is reduced to that of calculating the momentum-dependent dielectric function $\varepsilon(q, \omega)$. This problem has been widely studied but has been solved satisfactorily only for the case of a nearly free-electron gas (FEG). In this instance one may use the theory of Lindhard to define the resonant behaviour of a lossless FEG [7], or the theory of Mermin for a more physical description inclusive of excitation lifetime broadening [8]. The commonly used Drude model lacks any well-defined dispersion relation for low-energy electron excitations [20].

To calculate the IMFP we must determine the dielectric function or the ELF. The optical limit of the dielectric function $\varepsilon(0, \omega)$ and the optical ELF, $\mathrm{Im}\left[\frac{-1}{\varepsilon(0,\omega)}\right]$, may be obtained directly using optical transmission or reflection measurements [29,30], or inferred from electron energy loss spectroscopy (EELS) or reflection EELS [31–36]. Recent developments have also enabled calculations of the optical ELF using density functional theory (DFT) [18,20]. The optical data model asserts that the momentum-dependent ELF of a solid may then be determined by constructing a sum of FEG type resonances (Lindhard, Mermin, or otherwise) that match the optical behaviour of the material - i.e. the ELF in the limit $\hbar q \to 0$. Mathematically we can write this condition as

$$\mathrm{Im}\left[\frac{-1}{\varepsilon_{\mathrm{data}}(0,\omega)} \right] = \sum_i A_i \mathrm{Im}\left[\frac{-1}{\varepsilon_{\mathrm{FEG}}(0,\omega;\omega_p = \omega_i)} \right] \tag{6}$$

where $\mathrm{Im}\left[\frac{-1}{\varepsilon_{\mathrm{FEG}}(0,\omega;\omega_p=\omega_i)}\right]$ is the optical loss function for a free-electron gas. This loss function will consist of a single resonance peak, situated in the optical limit at the plasma frequency $\omega_p = \omega_i$. The relative amplitudes A_i are defined by the match to the externally determined optical spectrum. If Lindhard-type functions are used to define the FEG, then each component resonance will be a delta function in the optical limit, and the A_i terms are uniquely defined:

$$A_i = \frac{2}{\pi\omega_i} \Delta\omega \mathrm{Im}\left[\frac{-1}{\varepsilon_{\mathrm{data}}(0,\omega_i)} \right] \tag{7}$$

where $\Delta\omega$ is the spacing between sampled points on the externally-determined optical spectrum. If we then sum such component resonances using their full momentum-dependent forms, we arrive at a momentum-dependent ELF for the solid:

$$\mathrm{Im}\left[\frac{-1}{\varepsilon(q,\omega)} \right] = \sum_i A_i \mathrm{Im}\left[\frac{-1}{\varepsilon_{\mathrm{FEG}}(q,\omega;\omega_p = \omega_i)} \right] \tag{8}$$

In this way we can extend the FEG theory to describe the behaviour of a real solid with complex band structure. If $\varepsilon_{\mathrm{FEG}} = \varepsilon_{\mathrm{L}}$, so that each resonance in the optical limit is a Lindhard resonance, a delta function, then the extension into q-space is given uniquely and exactly by: [7]

$$\varepsilon_L(q,\omega) = 1 + \frac{3\omega_p^2}{q^2 v_F^2} f \tag{9}$$

$$v_F = \frac{\hbar}{m} \left(\frac{3\pi^2 m \omega_p^2}{e^2} \right)^{1/3} \tag{10}$$

$$f = \frac{1}{2} + \frac{1}{8z}[1 - (z-u)^2] \ln\left[\frac{z-u+1}{z-u-1} \right] + \frac{1}{8z}[1 - (z+u)^2] \ln\left[\frac{z+u+1}{z+u-1} \right] \tag{11}$$

$$u = \frac{\omega}{q v_F};\ z = \frac{q}{2q_F};\ \omega_F = E_F/\hbar;\ q_F = \sqrt{2mE_F}/\hbar;\ \omega_p = \sqrt{\frac{4\pi n e^2}{m}} \tag{12}$$

with the Fermi velocity v_F and Fermi wave vector q_F defined in terms of the Fermi energy E_F and the Fermi frequency ω_F. This is much more complex than the approximate q-space extensions of Eqs. (2) and (3). The use of Lindhard terms to construct the electron ELF has become a common practice, because it is uniquely constrained via Eq. (7) and because it can be used to match any optical dielectric function precisely. To understand this note that any spectral function in the optical limit is uniquely decomposed into an infinite sum of Dirac delta functions and amplitudes (i.e. source terms for the Lindhard functions), so that this prescription is always possible and always unique. The great success of the 1980s was the development by Penn of the Penn algorithm to define the IMFP explicitly and uniquely in terms of the optical

data limit, the representation of these as a sum of delta-function Lindhard functions, and the consequent extension into q-space [14].

$$\lambda(E)^{-1} = \frac{\hbar}{a_o \pi E}\int_0^{\frac{E-E_F}{\hbar}}\int_{q_-}^{q_+}\int_0^{\infty}\frac{2}{\pi\omega' q}\mathrm{Im}\left[\frac{-1}{\varepsilon_{\mathrm{data}}(0,\omega')}\right]\mathrm{Im}\left[\frac{-1}{\varepsilon_L(q,\omega;\omega_p=\omega')}\right]d\omega' dq d\omega \quad (13)$$

This is an archetypal example of a Partial Pole Model - the optical limit spectrum is represented as an infinite sum of delta functions for each $\omega_p = \omega$, and each of these is propagated as an independent pole (or Lindhard function) into q-space. It is called a Partial Pole Model because the optical limit resonance, i.e. the corresponding plasmon in the optical limit, may not have zero width and therefore the pole or plasmon would be subdivided into a set of partial poles for each plasmon resonance. Indeed the dielectric function for a photon (the optical limit) has lifetimes of excited states in pure absorption following the quantum mechanical decay process, so it is sensible to define this approach as a partial pole approach.

This approach has been developed over some decades from the original works of Penn [14] and Tung et al. [37]. A version of this model is used in the work of Tanuma et al., who have constructed the most comprehensive and widely-cited tabulations of IMFPs in the current literature [25].

This can then be integrated following (4) to evaluate the electron IMFP. The Lindhard model is, however, unphysical due to its lack of broadening to account for the lifetime of the excitations it represents. Similarly, the Penn algorithm fails because it is lossless: plasmons have finite lifetimes and hence IMFPs too!

This limitation of the Lindhard function led to the development of the Mermin function [8], which expands on the Lindhard function to include a lifetime broadening parameter γ in such a manner that it retains adherence to the causal constraints of the Thomas-Reiche-Kuhn and Kramers-Kronig sum-rules [38]. The Mermin dielectric function, $\varepsilon_M(q, \omega, \gamma)$, is defined in relation to the Lindhard dielectric function, $\varepsilon_L(q, \omega)$, by

$$\varepsilon_M(q,\omega,\gamma) = 1 + \frac{(1+i\gamma/\omega)[\varepsilon_L(q,\omega+i\gamma)-1]}{1+(i\gamma/\omega)[\varepsilon_L(q,\omega+i\gamma)-1]/[\varepsilon_L(q,0)-1]} \quad (14)$$

where γ is the broadening associated with the finite lifetime of a resonant excitation. The use of Mermin terms in the optical data model has become popular only in recent times [17,39,40], and has been used to demonstrate that the observed discrepancies between theoretical and experimental IMFPs may be reduced significantly by the inclusion of plasmon broadening terms γ_i [41]. These Mermin-based optical data models are, however, still subject to a number of limitations in terms of both implementation and physicality.

In particular, Mermin-based optical data models may be Partial Pole models (with delta functional in the optical limit, like the Lindhard functions, so that the optical limit data is still uniquely defined as a sum of delta functions), or Many Pole models (with resonance widths in the optical limit being non-zero and often attempting to mimic the widths observed in the optical data or in the theoretical computation). Unfortunately, there has been no unique or robust way to calculate γ, only empirical fitting algorithms. A key set of assumptions in the past literature, which we think have now been disproven, include the hypothesis $\gamma(i, q, \omega) = \gamma$, constant, $\forall i, q, \omega$. Clearly different upper levels or excited plasmons will have different lifetimes. The hypothesis $\gamma(i, q, \omega) = \gamma_i$, constant for each i, $\forall q, \omega$, has also been rejected, as the lifetime should certainly depend upon the electron momenta and vector in a band structure. And similarly, the hypothesis $\gamma(i, q, \omega) = \gamma_i(\omega)$, constant for each i, ω, $\forall q$ is also improbable.

Whilst the Penn algorithm can be applied uniquely and universally to any optical data, it has been recognised that one of the key problems of any free electron gas model including the Lindhard and by extension the Penn, is the solid state structure due to band theory and in particular the band gap E_g for any semiconductor, for example. For this purpose the Levine-Louie function was developed [13], which is a partial pole model defined in terms of lossless Lindhard functions, as:

$$\varepsilon(q,\omega) = \varepsilon_L(q,\omega_-), |\omega| \geq E_g/\hbar;\ \mathrm{Im}(\varepsilon(q,\omega)) = 0,\ |\omega| < E_g/\hbar; \quad (15)$$

$$\mathrm{Re}(\varepsilon(q,\omega)) = 1 + \frac{2}{q_F a_0 \pi}\left[\frac{1}{Q^2} - \frac{\Delta}{2Q^3}\left[\tan^{-1}\frac{2Q+Q^2}{\Delta} + \tan^{-1}\frac{2Q-Q^2}{\Delta}\right] + \left[\frac{\Delta^2}{8Q^5} + \frac{1}{2Q^3} - \frac{1}{8Q}\right]\ln\left\{\frac{\Delta^2+(2Q+Q^2)^2}{\Delta^2+(2Q-Q^2)^2}\right\}\right],\ |\omega| < E_g/\hbar \quad (16)$$

$$Q = q/q_F;\ \Delta^2 = \lambda^2 - \omega^2/\omega_F^2;\ \lambda\omega_F = E_g/\hbar;\ \omega_-^2 = \omega^2 - (\lambda\omega_F)^2 \quad (17)$$

This is a truncated Lindhard function with no possible absorptive component for plasmons within the band gap; however, if the only plasmons are above the band gap then this modification and the corresponding transform do nothing, and one might as well start with the Lindhard functions but only allow non-zero components above the band gap energy. Because each component is a delta-function, the implied lifetime of the plasmon remains infinite and non-causal. In a similar vein, a more appropriate functional for conductors has been proposed by Tung et al. to address deficiencies of the free electron gas approach relative to solid state band structure, following a Drude approach but with a double summation over conduction electrons and plasmons ($\omega_i = 0$) and over valence and related resonances ($\omega_i \neq 0$) [37,42]. This is a many-pole model. More recently there has been a development of tabulations based upon these principles and perhaps a question of the separation of plasmon excitations and interband transitions. An example of the difference in the energy loss spectrum using typical Mermin parameters for a single resonance compared with a partial pole sum of Lindhard terms is given in Fig. 1, with the Mermin result shown in 3D in Fig. 2.

The understanding of the electron IMFP is critical for spectroscopies that involve primary or secondary electron probes, including e.g. Electron Energy Loss Spectroscopy (EELS), Electron Diffraction, Electron Microscopy (LEEM, PEEM, ...), and overlayer experiments. The importance of low-energy IMFP for electron particle transport, detector modelling, EPES, XPS and related spectroscopies has been emphasised [43–45].

3. Applications to X-ray absorption and measurements via the X-ray extended range technique

X-ray Absorption Spectroscopy (XAS) yields a secondary low energy photoelectron which produces an interference wave with the returning elastically scattered electron, and thus directly probes properties of electrons, plasmons and IMFPs particularly below 200 eV. One of the best techniques for high-accuracy XAS is the X-ray Extended Range Technique (XERT) developed by our group [46,47]. All XAS techniques probe local structure and dynamics, and can be used as fingerprints for oxidation state, local geometry and dynamics, and dynamical bond lengths. This is especially good for local structure of partially disordered systems, even in solution or gas phase.

However, it has been important to us to look at current or perceived limitations of XAS. For example, can XAS measure accuracies in attenuation coefficients, absorption coefficients and X-ray absorption fine structure below 0.2%? The answer is Yes: in our absolute measurements we have achieved accuracies of these coefficients to 1×10^{-4} [48,49]. Can XAS measure bonding or nearest neighbour distances to better than

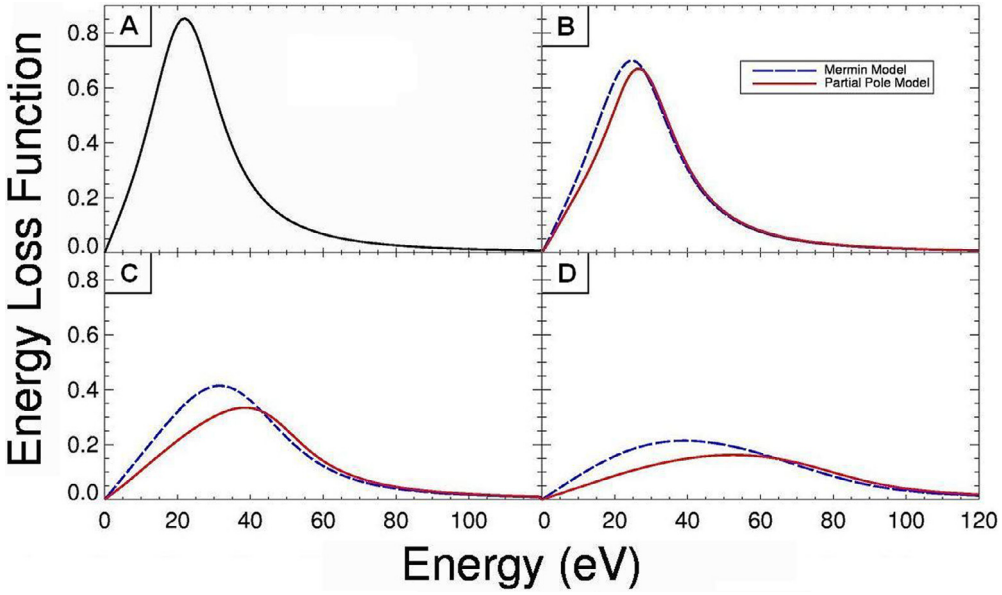

Fig. 1. One-component Mermin electron energy loss function for $A_i = 0.8$, $\gamma_i = 25\ eV$, $\omega_i = 25eV$ from A) $\hbar q = 0$ Å^{-1}, the optical limit; to B) $\hbar q = 1$Å^{-1}; C) $\hbar q = 2$Å^{-1}; and D) $\hbar q = 3$Å^{-1} compared to an equivalent Lindhard partial pole representation. The blue curve utilises a Mermin model extension, while the red curve (online in colour) uses a partial pole representation. The two models coincide in the optical limit. (For interpretation of the references to colour in this figure legend, the reader is referred to the web version of this article.)

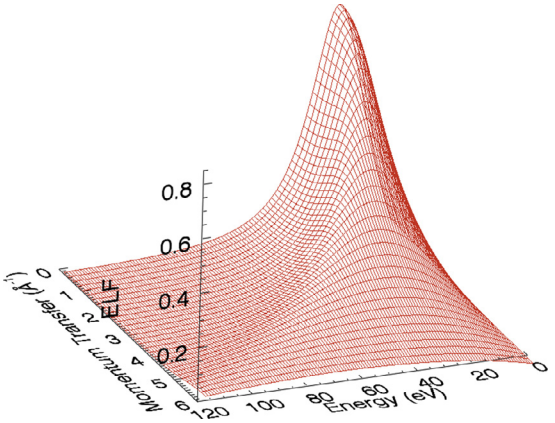

Fig. 2. One-component Mermin one-component electron energy loss function for $A_i = 0.8$, $\gamma_i = 25\ eV$, $\omega_i = 25eV$.

0.02 Å noting that errors in E_0 of 10 eV can shift bond lengths by 0.02 Å? Some highly accurate differential measurements have reported shifts of bond lengths $\delta r(T)$ of small values, but can absolute measurements be made down to these levels? Again the answer is Yes: Bonding has been measured in Mo, Au to 0.1% or 0.002 Å. How does this compare with the determination of lattice spacings from X-ray crystallography of single crystals? On the same 'real systems' from crystallography, the accuracy claimed is similar, namely 0.1% i.e. 0.002 Å.

In other words, high-accuracy XAS, for example using XERT, is a sensitive probe of local order, local disorder, and dynamics and can compete or be complementary with many other current techniques [50–52]. Often our uncertainties and accuracies are 100 × smaller than previous literature [50]. This realisation spurred us to ask: If so, What is Possible? What new science, physics, chemistry can we discover? Until recently, this was constrained by limitations in XAS theory, in part based on muffin-tin potentials, and in part based on limitations of our modeling of electron transport properties and in situ dielectric response.

3.1. Full-potential theory and finite difference models for X-ray absorption

With our new full-potential theory [53], we can investigate the photoelectron interference pattern without fitting parameters for simple materials, such as copper, demonstrating that accurate experiment and accurate theory can agree [54–57]. This has a density functional theory core (DFT), using a local density approximation with Hubbard corrections for correlations, and time-dependent DFT (TD-DFT) for excited state functions via the WIEN2k package. In standard analysis, we can investigate structural parameters of molecules and fit down to $k = 1$ Å^{-1}. This, for example, has allowed us to discriminate between conformation states in organometallic catalysts, a dramatic breakthrough in sensitivity and insight [58]. Such developments allow us to see directly the impact of the previous theoretical predictions of the inelastic mean free path on the XAS spectrum, effectively via the XAFS equation:

$$\chi(k) = \sum_j N_j S_0^2 F_j(k) \frac{\sin(2kr_j + \phi_j(k))}{kr_j^2} e^{-2\sigma_j^2 k^2} e^{-2r_j/\lambda_j(k)},\ k = \frac{2\pi}{h}\sqrt{2m_e(E - E_0)} \tag{18}$$

Here the amplitude of the interference oscillations $\chi(k)$ is given by a sum over paths r_j to all electron density (or each atomic position) with degeneracy N_j, many-body reduction factor S_0^2, magnitude of the scattering factor $F_j(k)$, phase offset for the path and scattering ϕ_j, thermal (Debye or disorder) broadening σ_j^2 and inelastic mean free path $\lambda_j(k)$.

Notice particularly that the IMFP is a function of the photoelectron k, so that although the energies of the X-ray or inner shell binding are large, the XAFS just above the edge has a very low-energy photoelectron energy and momentum, so that the information provided is of the explicitly low-energy electron IMFP. Notice also that the elastic scattering, which is almost indistinguishable in some other experimental techniques from the inelastic scattering, is here fully orthogonal. Elastic scattering strengthens the interference amplitude, while inelastic scattering weakens and dampens the interference amplitude observed experimentally. This equation is currently used in over 90% of all XAFS analysis by: path-integral integration over atomic sites (maximum electron density and scattering); or shell-integral approaches of radial density or peaks; or Green's function integrals of higher-order

interactions. However, the interference is really a spatial and orientation-specific integral over the potential throughout space, both at atomic locations but more generally wherever the electron density and the change of potential is a source term for scattering. In that sense non-muffin-tin approaches such as FDMNES and FDMX [53] are part of the new generation of computational approaches; but the basic idea remains valid. Because of the very good agreement of the experimental data and theory, the more subtle broadening due to the IMFP became obvious [56].

Whereas established techniques for IMFP measurement tend to become far less accurate at low energies (below a few hundred eV) due to elastic scattering and surface effects, X-ray Absorption Fine Structure (XAFS) is a unique electron spectroscopy that explicitly separates the effects of elastic and inelastic photoelectron scattering in the photoabsorption spectrum just beyond an ionization edge. Fundamentally, the elastic scattering increases the backscatter and the strength of the interference, while the inelastic scatter dampens the interference as a function of energy or electron momentum and distance to the scatterer. From the previous equation, inelastic scattering causes an energy-dependent broadening of the XAFS:

$$\Gamma(E) = \frac{\hbar}{\lambda(E)}\sqrt{\frac{2E}{m}} + \Gamma_H \tag{19}$$

or equivalently, dampens the photoelectron wave-function, modulating its self-interference. Here Γ_H is the (intrinsic) holewidth of the Lorentzian lifetime of the inner-shell hole state. Given a sufficiently accurate experiment, and sufficiently robust theory, one can extract the IMFP from XAFS data.

4. [Photo-] electron inelastic mean free paths - surprising results from XAS measurements

A particularly striking example of the value of XAS measurements to electron transport theory comes from analysis of results for elemental copper [59]. The experimental data for copper has uncertainties of approximately 0.15%–0.30% in the energy range of interest, which is highly accurate in this field (usually accuracies are 1%–3%). Fig. 3 demonstrates the sensitivity of our approach to different theoretical models for the IMFP, and shows that there are substantial discrepancies

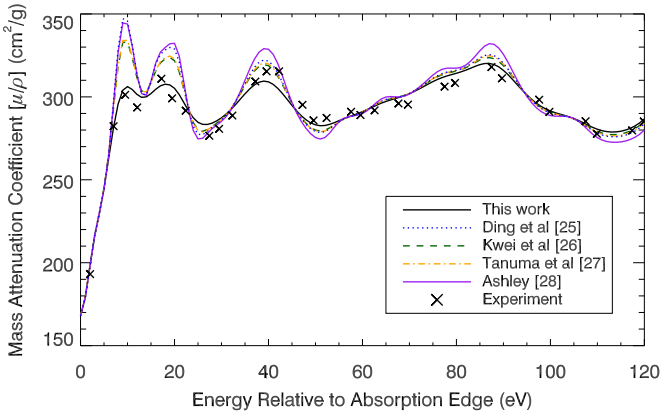

Fig. 3. Mass attenuation coefficients for copper calculated using different tabulations for the IMFP, compared with experiment [59]. The results are particularly sensitive to the IMFP at low energies. Earlier theories are severely inconsistent with experiment in this region. Experimental modelling results (solid black curve) are from Bourke et al. [16]. Notice that the modelling function follows the data extremely well above about 40 eV and that the broadening is well-defined here. At low energies, whilst the alternate works are far too narrow, the modelling prescription produces greatly improved interference magnitudes. Residual errors in the complex shape of the XAFS spectrum are primarily due to limitations in XAFS theory, and allow for some additional uncertainty in the fitted IMFP.

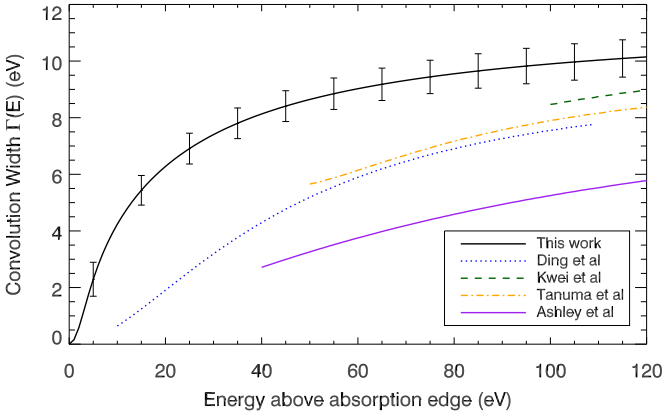

Fig. 4. Width of the Lorentzian curve to be convolved with the calculated X-ray absorption spectrum of copper, in order to account for the effect of the finite IMFP. This curve is produced by fitting the resultant convolved spectrum with experimental data [59,63]. Also shown are the three-standard-deviation fitting uncertainties, absent potential model-dependent inaccuracies. The colored curves represent the broadening associated with literature calculations, which are highly inconsistent with one another and with the fitted result.

between competing theories at low energies. Also clear is the need for a more realistic account of the IMFP below 30 eV, where there exists no IMFP calculation that leads to adequate agreement with the experimental data [16].

Fig. 4 shows the required convolution width for the IMFP correction in copper, while Fig. 5 shows the resulting IMFP values, with uncertainties. These are three standard deviation uncertainties determined by our fitting procedure based on the propagation of uncertainties from the experimental error bars. Figs. 4 and 5 also give theoretical values calculated by Ding et al. [60], Kwei et al. [42], Tanuma et al. [61] and Ashley [62]. All use variations of the common optical data model presented by Penn [14].

Established theories appeared to overestimate the IMFP below 120 eV, so this raises a question as to what a valid theory is and how do the existing theories need to be reevaluated? This led us to an investigation of the causal requirements of a theory of plasmons.

Models of the electronic response in condensed-matter systems are usually derived from free-electron gas or jellium models, which

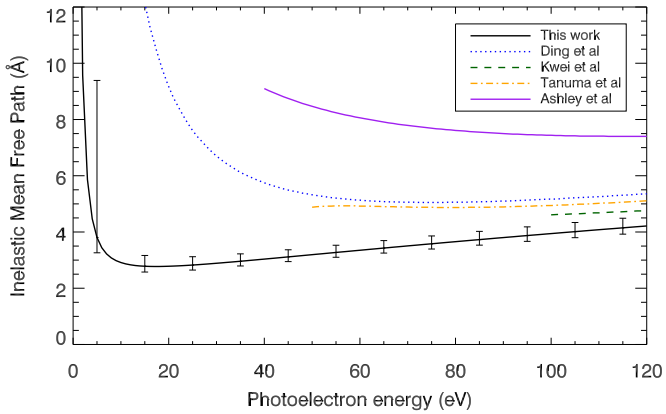

Fig. 5. The Inelastic Mean Free Path (IMFP) for copper from X-ray Absorption Fine Structure (XAFS) measurements, with three standard deviation error bars [16] and previous theoretical calculations of the IMFP from various sources. Significant deviation is seen in the low energy region, as expected. Although low energy data is not available from the multiple-pole calculation [42], it agrees best with our results as the energy drops to 100 eV. Below about 150 eV, we see that the IMFP appears to be lower than previously thought. At energies below 40 eV, model-dependent effects could plausibly increase the fitted values, but are unlikely to bring them close to the plotted theories.

commonly neglect to account for the lifetime broadening of individual plasmon and single-electron excitations in a constrained, physical manner. This can lead to potentially significant errors in electron energy loss spectra and electron inelastic mean-free-path (IMFP) calculations. Even when broadening parameters are included in Drude or Mermin-type models, they are almost always held as constants even though the lifetime broadening of a plasmon or single-electron excitation is, in fact, likely to be variable based on its energy and momentum [28,64]. The inclusion of the broadening term γ_i also complicates the [optical limit] data-matching procedure. When $\gamma_i = 0$, δ functions may be uniquely defined with amplitudes matching the optical ELF data. With excitations of finite width, however, there potentially exist many possible ways to fit the optical spectrum, and thus the parameters A_i, ω_i, γ_i are not uniquely defined. This results in a large range of potential values for the ELF at high values of momentum transfer q.

5. Excitation broadening and sum-rules

These problems may be addressed with the implementation of a momentum-dependent lifetime $\gamma_i(q)$ assigned to each excitation. To provide any valid model, it must be constrained by (causal) sum rules [38]. The Thomas-Reiche-Kuhn rule, also commonly known as the *f*-sum rule, is given by

$$\frac{\pi}{2}\omega_i^2 \approx \int_0^\infty \omega \mathrm{Im}\left[\frac{-1}{\varepsilon(\omega)}\right] d\omega \tag{20}$$

This rule is generally applicable to all values of momentum transfer $\hbar q$, and is commonly used to evaluate the consistency of measured and calculated optical dielectric data [20]. This expression applies to a single oscillator, or a free-electron gas with a well-defined resonance frequency ω_i. For a general material with several resonance peaks, the plasma frequency must be replaced using $\omega_i = \omega_P = (4\pi n e^2/m)^{1/2}$, where n is the (local or effective) density of electrons in the material. In any Lindhard model or in a Dirac-delta function optical limit model, this is a direct integral of delta-functions across the available range of energies for possible plasmon contributions (see below, Eqn 13, Eqns 38, 39). If any optical data is already compliant with the *f*-sum rule, then we need only ensure that the value of the *f*-sum, defined by the right-hand side of Eq. (20), is self-consistent across all momenta.

The Kramers-Kronig, or KK-sum rule, is given by

$$1 + \mathrm{Re}\left[\frac{-1}{\varepsilon(q,0)}\right] = \frac{2}{\pi}\int_0^\infty \frac{1}{\omega}\mathrm{Im}\left[\frac{-1}{\varepsilon(q,\omega)}\right] d\omega \tag{21}$$

Whereas the *f*-sum rule relates to the integral of the oscillator strengths or equivalently the number of electrons per volume in the solid, the KK-sum rule is a statement of causality as the dielectric function must be a self-consistent complex function with the real component directly related to the imaginary component. This rule is also applicable across all momenta, however the left-hand side of the expression can be ill-defined for $q \neq 0$. We therefore make an approximation following the Drude dielectric theory, which represents the real component of the inverse dielectric function in terms of ω_q, the resonant or peak energy of an excitation at momentum $\hbar q$ [42]:

$$\mathrm{Re}\left[\frac{-1}{\varepsilon(q,0)}\right] \approx \frac{\omega_i^2}{\omega_q^2} - 1 \tag{22}$$

This allows us to re-write the KK-sum rule as

$$\frac{\pi}{2}\omega_i^2 \approx \omega_q^2 \int_0^\infty \frac{1}{\omega}\mathrm{Im}\left[\frac{-1}{\varepsilon(q,\omega)}\right] d\omega \tag{23}$$

where again we find a constraint that the right-hand side of the expression must remain constant across all momenta. In general, the behaviour of an excitation typically follows some kind of dispersion relation, whereby the resonant energy of the excitation is related to its momentum following some functional form g such that

$$\omega_q = g(q, \omega_i) \tag{24}$$

A simple approximation for g, sometimes used in Drude theories, is that of a free particle:

$$g(q, \omega_i) = \omega_i + \frac{\hbar q^2}{2m} \tag{25}$$

which is consistent with Eq. (2) in the trivial case of $\alpha = 1$. Whatever form g may take, it is apparent that as the energy of the excitation changes with its momentum, so too must its amplitude change in order to continue to satisfy the sum rules. Further, whatever functional form one takes for the ELF of the free-electron gas component, this change in amplitude must counteract an equal change in both the *f*-sum and KK-sum values. We therefore infer the following condition for any model of the dielectric function:

$$\frac{\int_0^\infty \omega \mathrm{Im}\left[\frac{-1}{\varepsilon(0,\omega)}\right] d\omega}{\int_0^\infty \omega \mathrm{Im}\left[\frac{-1}{\varepsilon(q,\omega)}\right] d\omega} = \frac{\omega_i^2 \int_0^\infty \frac{1}{\omega}\mathrm{Im}\left[\frac{-1}{\varepsilon(0,\omega)}\right] d\omega}{\omega_q^2 \int_0^\infty \frac{1}{\omega}\mathrm{Im}\left[\frac{-1}{\varepsilon(q,\omega)}\right] d\omega} \tag{26}$$

This expression may be simplified further for any model that represents resonances in the optical limit as delta functions. Although it is generally unphysical for a resonance to correspond to a delta function due to its implied infinite lifetime, such a modelling is not necessarily unphysical as the optical limit is itself an idealisation, existing in the realm of zero momentum. A model which constrains $\gamma_i = 0$ in the optical limit may still include finite lifetime resonances for finite momenta, and can also be used to uniquely parameterise the optical ELF following (6). For such a model, we may write the following powerful condition constraining the dielectric function [65]:

$$\frac{1}{\omega_q}\int_0^\infty \omega \mathrm{Im}\left[\frac{-1}{\varepsilon(q,\omega)}\right] d\omega = \omega_q \int_0^\infty \frac{1}{\omega}\mathrm{Im}\left[\frac{-1}{\varepsilon(q,\omega)}\right] d\omega \tag{27}$$

5.1. Symmetric rectangular broadening

We can use a simple example to illustrate how these sum-rule restrictions can be used to develop a formalism involving a q-dependent plasmon broadening width $\gamma(q)$. The simplest arbitrary form possible for a single plasmon resonance making up an ELF would be that of a rectangular function defined as follows:

$$\mathrm{Im}\left[\frac{-1}{\varepsilon(q,\omega)}\right] = \begin{cases} \frac{A_i}{\gamma_i \omega_q} & \text{for } \omega_q - \frac{\gamma_i}{2} < \omega \leq \omega_q + \frac{\gamma_i}{2} \\ 0 & \text{otherwise} \end{cases} \tag{28}$$

As before, A_i is a constant amplitude factor designed to match external data in the optical limit and γ_i is the plasmon width. ω_q is the q-dependent resonant energy for the plasmon pole given by a dispersion relation $\omega_q = g(q, \omega_i)$, where $\omega_q = \omega_i$ when $q = 0$.

In the optical limit, the ELF defined by Eq. (28) gives an *f*-sum rule result of A_i (RHS of Eq. (20)), and a KK-sum rule result of $\frac{A_i \omega_q}{\gamma_i} \ln \frac{\omega_q + \gamma_i/2}{\omega_q - \gamma_i/2}$ (RHS of Eq. (23)). Note that the *f*-sum rule result is entirely independent of both γ_i and q. In the limit of γ_i approaching zero, the KK-sum rule result also reduces to A_i, meaning that for a lossless excitation both the *f*- and KK- sum rules are consistent and independent of q. This of course is true for the Lindhard and related models, where $\gamma_i = 0$.

If γ_i is finite, then the KK-sum rule will retain its ω_q, and hence q, dependence. This means that a rectangular form for plasmon resonances can never satisfy Eq. (27), and therefore can never be self consistent for *constant and finite* broadening widths. This limitation applies to constant and finite widths in both the Drude and Lindhard dielectric theories.

This can be generalised to a variable width $\gamma_i(q)$ with a renormalisation factor $N_i(q)$ to no avail. A symmetric rectangular (broadening) function cannot satisfy the sum-rules as q increases [65]. A generalisation, not proven, is that the plasmon broadening for increasing finite momentum transfer *cannot be symmetric*.

5.2. Asymmetric rectangular broadening

An asymmetric broadening is the only way in which we can ensure that the effect of broadening, like the effect of the renormalisation factor $N_i(q)$, changes the outcome of the KK-sum rule and the outcome of the *f*-sum rule *by the same amount*. For our example plasmon equation, this means we must rewrite the equation as

$$\mathrm{Im}\left[\frac{-1}{\varepsilon(q,\omega)}\right] = \begin{cases} \frac{N_i(q)A_i}{\gamma_i(q)\omega_q} & \text{for } \omega_q - \alpha_i(q) < \omega \le \omega_q + \beta_i(q) \\ 0 & \text{otherwise} \end{cases} \tag{29}$$

where $\alpha_i(q) + \beta_i(q) = \gamma_i(q)$, and $\alpha_i(q) \neq \beta_i(q)\ \forall\ q \neq 0$. The aim is then to construct $\alpha_i(q)$ and $\beta_i(q)$ so that the broadening they invoke affects the two sum rules equally, thus ensuring satisfaction of Eqs. (26) and (27) for all values of q. We define the renormalisation factor as

$$N_i(q) = \frac{\int_0^\infty \omega \mathrm{Im}\left[\frac{-1}{\varepsilon(0,\omega)}\right] d\omega}{\int_0^\infty \omega \mathrm{Im}\left[\frac{-1}{\varepsilon(q,\omega)}\right] d\omega} \tag{30}$$

Since we have defined an explicit form for our excitations (Eq. (29)), we can substitute into Eq. (27) to find an expression for the width parameters $\alpha_i(q)$ and $\beta_i(q)$:

$$1 + \frac{\beta_i(q)^2 - \alpha_i(q)^2}{2\omega_q(\alpha_i(q) + \beta_i(q))} = \frac{\omega_q}{\alpha_i(q) + \beta_i(q)} \ln\left(\frac{\omega_q + \beta_i(q)}{\omega_q - \alpha_i(q)}\right) \tag{31}$$

This relationship is satisfied by the trivial case of $\alpha_i(q) = \beta_i(q) = 0$, corresponding to a partial pole or lossless plasmon model [66]. Hence we have proven the self-consistency of the Lindhard model. We can also find an expression for $N_i(q)$ by combining Eqs. (29) and (30), yielding

$$N_i(q) = A_i\left[\omega_q + \frac{\beta_i(q)^2 - \alpha_i(q)^2}{2(\alpha_i(q) + \beta_i(q))}\right]^{-1} \tag{32}$$

We now have two equations (Eqs. (31) and (32)) and three unknowns ($N_i(q)$, $\alpha_i(q)$, and $\beta_i(q)$). We must therefore invoke a third constraint, which we will construct by relating the broadening parameter $\alpha_i(q)$ to the peak resonance energy $\omega_i(q)$. All of these options may be conveniently described by defining the following relationship between $\alpha_i(q)$ and $\omega_i(q)$:

$$\alpha_i(q) = \omega_q \frac{\omega_q - \omega_i}{\frac{\omega_i}{1 + a_i} + \omega_q - \omega_i} \tag{33}$$

We made three hypotheses to define the limits of parameter space:

1. $\alpha_i(q) = \beta_i(q) = 0$, 'a partial pole or lossless plasmon model' (e.g. Lindhard, symmetric): $\alpha_i(q) = 0$, for all q. i.e. $a_i = -1$

2. 'electronic excitations will propagate only at energies higher than the plasma frequency' $\omega_p = \omega_i(0)$: $\alpha_i(q) = \omega_q - \omega_i$. i.e. $a_i = 0$. This moderate broadening model in which excitations in the optical limit may result only in higher-energy excitations at finite momentum transfer, represents an approach similar, for example, to that of Sorini et al. [24].

3. 'excitations may exist below the plasma frequency' $q > 0$, $\alpha_i(q) > \omega_q - \omega_i$. e.g. $a_i = 100$. Resonances broaden to encompass energies both above and below the plasma energy of the material. This latter behaviour is qualitatively consistent with what may be expected in a Mermin model.

Among these models, it is found that none reproduce satisfactorily the experimental results of the previous sections across all energies, but rather that they align reasonably with experimental results within different energy regimes [65]. This implies that the level of broadening must be explicitly constrained in an energy-dependent fashion in addition to the momentum-dependence given by our sum-rule analysis. Further, while it may be expected that an asymmetric rectangle is not a physical model for broadening a spectrum into q-space from the optical limit, a key principle is that any alternative oscillator form must also be asymmetric.

The Mermin function can comply with the sum rules and therefore is an excellent example of a possible asymmetric broadening model. Alternatively, one might adapt the Lindhard functional using $u \to u' = \frac{\omega + i\gamma_i(q)}{v_F}$. This broadens the plasmon resonance, but does not preserve the local electron number density in the ELF and ergo breaks the Kramers-Kronig sum-rule. The Mermin functional normalises this, preserves the KK and *f* sum-rules $\forall\gamma_i$, reduces to the Lindhard model for $\gamma_i \to 0$, and reduces to the Drude model for $q \to 0$.

However, the optical limit data can arise from a variety of experiments and a wider variety of theoretical (usually density functional theory) models. The experimental data can be matched exactly to a partial pole model or fitted with or without uncertainties to an enormous array of many pole or multiple pole models. In the latter case the experimental or theoretical optical limit data is approximated in various ways with different resulting IMFPs.

Also, the degrees of freedom imply that a potentially infinite number of Mermin models can fit a given optical limit data set yet with extremely different predictions as to the IMFP and other low energy electron properties.

Mermin fitting approaches also suffer from physical limitations. For instance, the representation of the electron oscillators usually involves the use of a single broadening parameter γ_i for each excitation. In reality, the lifetime of an excitation is dependent not only on its energy but on its momentum, and so the use of a single parameter for this purpose is insufficient. A small number of works have investigated this problem, but without a clear physical guidance on the quantitative momentum-dependence of the broadening [64].

An even more severe problem is the initial assumption used in all optical data models that the solid is a sum of non-interacting FEG resonance terms. Clearly all of the electrons in a solid can interact, and therefore each excitation channel must be affected by all of the other resonances of the material.

5.3. The coupled-plasmon model

In light of these limitations, we have presented a new model based on a self-consistent Mermin representation with momentum-dependent broadening widths $\gamma_i(q)$ [19]. The first step, as in all optical data models, is to determine the spectrum at $\hbar q = 0$. To solve the problems of uniqueness and precise spectrum matching, we defined the following condition for all excitations *i*:

$$\lim_{q\to 0}\gamma_i(q) = 0 \tag{34}$$

This reduces the optical behaviour to the equivalent of a Lindhard model, uniquely constrained by Eq. (7). As suggested earlier, this reduction to Lindhard behaviour is permissible as the optical limit is an idealisation that does not apply to any real physical (electronic) system. Moreover, such a reduction is actually *predicted* by a self-consistent dielectric model.

The next problem is to specify the form of the values for $\gamma_i(q)$. For each optical component, we define a Mermin function which therefore obeys all the sum-rules and extensions into q-space. We then assert that the lifetime of each excitation is determined by the probability of it transferring energy into *other* valid excitations with magnitudes determined by their relative oscillator strengths. This approach solves not only the problem of specifying $\gamma_i(q)$, but also the problem of accounting for interactions between excitation channels, because it explicitly quantifies the coupling of the plasmon oscillations. We have seen that, for a free particle, an IMFP may be evaluated using Eq. (4). We may readily use the same formalism to derive an effective IMFP for a bound particle, provided we assign appropriate limits to the momentum integral. In this case, we use the standard relationship $\frac{\hbar^2 q^2}{2m} = \hbar\omega$ to generalise the expression for new momentum limits $q^* \pm$ to

$$q^* \pm = \sqrt{\frac{q^2}{\hbar\omega}E} \pm \sqrt{\frac{q^2}{\hbar\omega}(E-\hbar\omega)} \tag{35}$$

Given an effective IMFP, we can then infer a lifetime τ for the excitation by dividing the IMFP by the group velocity $\frac{d\omega_q}{dq}$. This derivative is evaluated based on the dispersion relation predicted by the Mermin formalism at the relevant point of energy and momentum. The lifetime τ is then inversely proportional to the broadening parameter $\gamma(\omega, q) = \hbar/\tau$, which we therefore define at any given combination of energy and momentum:

$$\gamma(\omega, q) = \frac{\hbar^2}{a_o \pi E}\frac{d\omega_q}{dq}\bigg|_{\omega,q} \int_0^{\omega-\omega_F} \int_{q_-^*}^{q_+^*} \frac{1}{q}\mathrm{Im}\left[\frac{-1}{\varepsilon(q,\omega')}\right] dq d\omega' \tag{36}$$

The width $\gamma_i(q)$ for a particular oscillator i is then related to this generalised broadening function following

$$\gamma_i(q) = \gamma(\omega_q, q) \tag{37}$$

with the special case at the optical limit of $\gamma_i(0) = \gamma(\omega_i, 0)$.

In the first instance, calculations are performed using a combination of Eqs. (4), (8) and (35), building an electron ELF using Lindhard-type FEG functions to approximate the behaviour of the solid. This computation is equivalent to the longstanding full Penn algorithm (FPA) [14], which forms the basis of several tabulations currently in the literature [25]. Values for $\gamma_i(q)$ are then obtained using Eq. (36) to define broadening widths for Mermin functions at all energies and momenta, and a new ELF is built using these functions. The process is then repeated until the electron ELF is converged and therefore self-consistent. Mathematically, we may define this iterative formalism by representing the inverse IMFP as a sum of broadened oscillators with relative strengths A_i:

$$\lambda(E)_N^{-1} = \frac{\hbar}{a_o \pi E}\int_0^{\frac{E-E_F}{\hbar}} \int_{q_-}^{q_+} \sum_i \frac{A_i}{q}\mathrm{Im}\left[\frac{-1}{\varepsilon_M(q,\omega,\gamma_i(q)_{N-1};\omega_p=\omega_i)}\right] dq d\omega \tag{38}$$

This equation can then be generalised by substituting an integral form of (7) to obtain

$$\lambda(E)_N^{-1} = \frac{\hbar}{a_o \pi E}\int_0^{\frac{E-E_F}{\hbar}} \int_{q_-}^{q_+} \int_0^{\infty} \frac{2}{\pi\omega' q}\mathrm{Im}\left[\frac{-1}{\varepsilon_{\mathrm{data}}(0,\omega')}\right]\mathrm{Im}\left[\frac{-1}{\varepsilon_M(q,\omega,\gamma_i(q)_{N-1};\omega_p=\omega_i)}\right] d\omega' dq d\omega \tag{39a}$$

$$\gamma_i(q)_N = \hbar\frac{d\omega_q}{dq}\bigg|_{\omega_q,q} \lambda(E)_N^{-1}\Theta(N-\delta) \tag{39b}$$

where the broadening values $\gamma_i(q)_N$ are given in terms of the IMFP $\lambda(E)_N$ by comparison with Eq. (36). Θ is the Heaviside step function and δ is a positive infinitesimal. Successive iterations of Eq. (39) generate a coupled-plasmon model of increasing order, with convergence to a self-consistent result typically achieved by $N > 4$.

This plasmon coupling theory [19] is then the first physical, uniquely constrained optical data model since the Penn algorithm [14]. Critically it has a similar unique match as the Penn model to any optical limit data, experimental or theoretical, by being a Partial Pole Model in the optical limit.

The theory computes explicit and individual $\gamma_i(q, \omega_i)$. It predicts greater broadening for higher momenta, because more lower-energy plasmon contributions will contribute to the higher energy broadening due to the plasmon coupling. It also predicts that in some cases plasmons below the plasma frequency can contribute significantly to the scattering of higher-energy plasmons. Since it calculates $\gamma_i(q, \omega_i)$ using the loss spectrum itself, it is also self-consistent once converged.

Some might prefer the Drude-type models, where the γ_i in the denominator, however determined, is exactly the Lorentzian broadening and is precisely the inverse of the lifetime. However, in that scenario the γ_i is usually unclear and its extension into q-space is even less clear. Similarly, the IMFP can be defined simply from the plasmon velocity and lifetime, so if optical data appears to have a specific resonance with a width of γ, then that should translate directly to equivalent lifetime and IMFP. In this self-consistent model, it does. If there is only a single isolated plasmon, approximating a δ-function, then simpler formalisms may be more-or-less effective. The error, perhaps, will be given by the magnitude of the coupling and broadening.

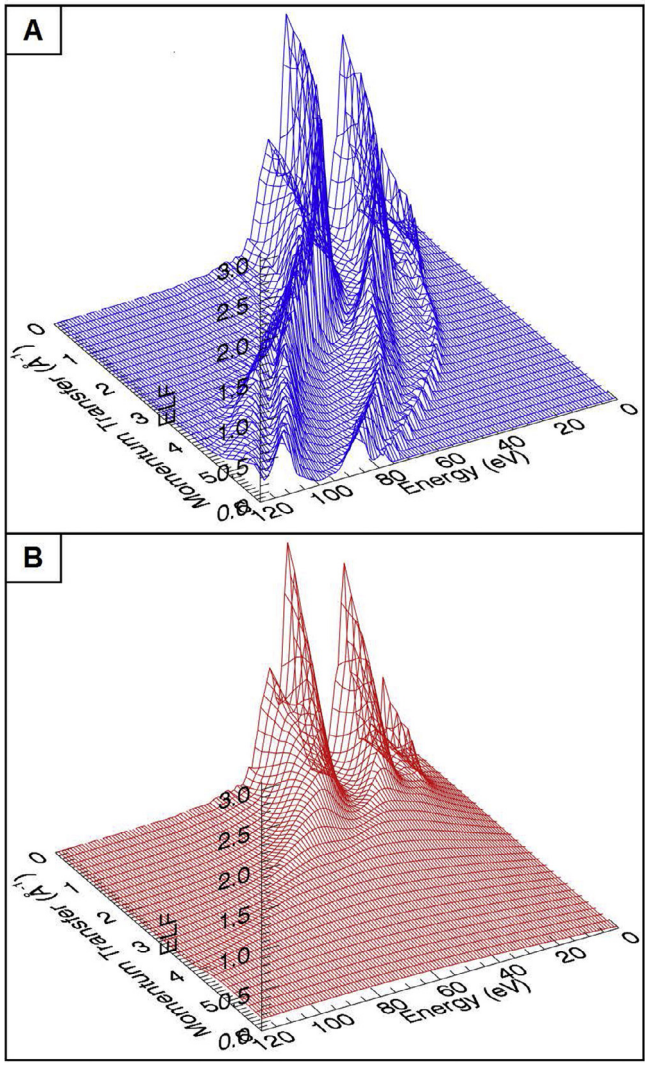

Fig. 6. The electron energy loss function (ELF) of elemental molybdenum. (A) is calculated using a lossless Lindhard model, while (B) utilises a self-consistent coupled-plasmon model (Eq. (39)) to incorporate excitation broadening.

Fig. 6 indicates the significance of the lifetime broadening and the plasmon-coupling to the ELF of metallic Mo. In a qualitatively similar fashion to previous Mermin-type modelling [41], the broadened ELF has less structure at high momenta and predicts greater scattering losses at low energies, leading to a lower electron inelastic mean free path (IMFP). The impact of the coupled plasmon model, and broadened models in general, is much more pronounced when the plasmons have structure than when there is a single narrow plasmon (e.g. Mo versus Al in Fig. 7). The implementation of self-consistent excitation broadening has a dramatic effect on the IMFP for molybdenum due to its broad loss spectrum and many excitation channels, while the reduction for aluminium is far more modest due to its singly-resonant loss structure. To summarise: The introduction of the coupled plasmon model makes a

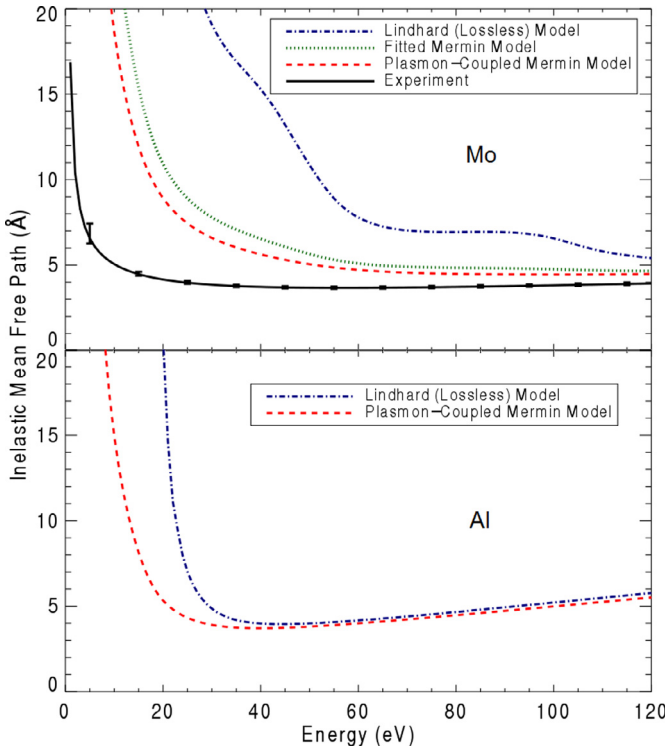

Fig. 7. Theoretical and experimental determinations of the electron IMFP for molybdenum and aluminium. The solid black curve with uncertainties shows a recent high-precision Mo measurement from XAFS [19], while the green dotted curve uses a more traditional fit-based Mermin modelling. The blue dot-dashed curves show results from a lossless Lindhard type representation of the electron ELF, while the red dashed curves use the current coupled-plasmon model defined by Eq. (39). (For interpretation of the references to colour in this figure legend, the reader is referred to the web version of this article.)

major improvement and a correction by up to 50% or more, from 0 to 120 eV and above, on the results from a Lindhard model. Compared to one of many (advanced) Mermin models the improvement is perhaps 30% or more below 60 eV or so but is still significant and 10–20% up to and above 120 eV, in part explicitly due to coupling. Conversely, for an ideal simple system such as aluminium where there is effectively only a single isolated plasmon, the coupled plasmon model make a mild improvement compared with Lindhard models; and most of this improvement is due to the lifetime broadening of an advanced self-consistent Mermin model rather than particularly due to coupling of the plasmons. Again to summarise, the coupled plasmon model is very important for all models where the is more than one plasmon, isolated or overlapping; and the use of a finite lifetime for the plasmon away from the optical limit is almost always essential.

Another area of useful insight on plasmon models relates to the investigation of the Bethe Ridge (or Bethe Surface) [27]. It has been used to guide and constrain dielectric models since 1930. The original idea was that the high-momentum limit should correspond to a classical free particle:

$$\lim_{q\to\infty}\omega_q = \frac{\hbar q^2}{2m} \tag{40}$$

Recent work has shown that the dispersion relation at intermediate energies is also extremely important for low-energy modeling and that the functional form has a significant impact upon the understanding of transport properties. For example, when an excitation only follows the Bethe Ridge at high momenta, then the rate of change of ω_q - which we understand as the group velocity v_g - will also be momentum dependent. It is therefore important to check that the theory also obey the energy conservation condition:

$$\lim_{q\to\infty}\int_0^q \frac{d\omega_q}{dq'}dq' = \lim_{q\to\infty}\int_0^q v_g dq' = \frac{\hbar q^2}{2m} \tag{41}$$

We find that in Lindhard-based models such as ours the low-energy excitations have a minimum lifetime broadening if $E = p^2/2m$, implying somewhat intuitively that free particles interact less strongly with the solid than bound states. More importantly, this is offset by a corresponding maximum lifetime broadening at higher momenta, meaning that the integral is able to recover the classical result of Eq. (41) at each energy transfer ω. Conversely, Drude quadratic and quartic extensions fail because they predict smoothly-varying group velocities that are always either higher or lower than the classical result, and therefore erroneously integrate to a total energy that is inconsistent with Eq. (41).

The coupled-plasmon theory makes new predictions for low energy electron transport in matter. Major differences are seen below 200–300 eV, with apparently improved agreement with experiment, and consequences for LEEM, PEEM, LEED, EELS, Monte Carlo and detector design. This is a constrained physical model of plasmon and single-electron excitations in a bulk solid. Interaction and coupling between different resonant excitations is included. High energy resonances couple to low energies, therefore yielding increased broadening, effective for all energies. The model explains a significant portion of observed discrepancies between theory and experiment in low energy electron IMFPs, and enables a robust and fully self-consistent theory with no free or fitted parameters that reveals additional physical insight not present in previous work.

6. Selected recent developments by other groups

Sorini et al. [24] in a series of publications have developed their tabulation / core theory from a single pole formalism for XAFS and IMFP to a multiple-pole formalism. They use a quartic Drude extension into q-space.

Use of Mermin functionals for representing the dielectric function and energy loss function have also been implemented by Denton et al. using a constant broadening for each oscillator [39]. This tabulation commented that Mermin has not previously been used because of the computational complexity. One of their key conclusions (with which we agree) is that Mermin functions, or causal broadening of plasmons, even if unconstrained and ill-defined, are far better than the use of loss-less functionals.

Werner et al. [20] have made major developments in IMFP theory and in particular have prepared a WIEN2K code for the DFT computation in the optical limit. In this work they use the Drude - quadratic extension with $\alpha = 1$ and $\alpha = 0.5$, in part on the basis of occupation number. Only the $\alpha = 1$ extension approaches the correct high-momentum Bethe ridge limit. These excellent works may need to consider the functional form of the q-space extension.

Da et al. [40] and related papers have looked at ways to take the Mermin formalism with finite (large) widths in the optical limit, and exactly match the experimental data. In pursuit of this they have used some 77 Mermin functions to fit the optical limit, including 37 negative oscillators, with arbitrary undefined widths to ‘fill’ optical data. This impressively achieves ‘perfect agreement’ with Chantler experiment - $\chi_r^2 = 0$ by empirical fit. However, while the negative oscillators help resolve the limitation of precise agreement with the optical limit, they generate a large number of unconstrained resonance terms, which in turn exacerbate another problem with the Mermin representation - that of uniqueness.

In recent papers, Nyugen-Truong [67–70] have implemented three variations of modeling and theory using Mermin functions. In all cases they report major improvement with the lifetime broadening and the Mermin extension into q-space. These models do not have a q dependence of the widths, and do not have plasmon coupling. However, they do find an important and similar improvement for their models with the

implementation of Mermin functions, and also provide insight into potential implementations of aspects of exchange and correlation for the dielectric response of the absorbing material. The key differences between a constant broadening for the Mermin function and equivalently a constant lifetime for the plasmons in q-space is that there is no change of shape with q, so that the behaviour can be a good first order or average correction across central plasmon frequencies and momenta. Hence it might be expected that dependencies from low E to higher E would change the functional form. de Vera and Garcia-Molina have an arXiv manuscript (2019), also using Mermin functions, also showing improvement compared with Lindhard functions, and noting the discrepancy with the experimental data for Cu from XAFS measurement [71].

Excellent recent work has been that of Vos and Grande [72–75] on experimental and theoretical modelling. They have detailed investigations of comparative theory, excellent complementary experiments; comment on the difficulty of separating surface from bulk plasmons; and discuss an explicit separation of plasmons from interband transitions. They introduce the Mermin-Levine-Louie function as a corresponding improvement over the Lindhard-based Levine-Louie functional.

Shirley has developed the 'Ocean Software', incorporating the electron-hole correlation of excitations [76,77]. This may have some important contribution to remaining discrepancies in IMFP and ELF modelling. And Tanuma, Powell, Penn continue to produce the benchmark new tabulations, references, and summaries of experiment for investigations on IMFP and other electron transport properties.

7. Conclusions

Recent work has clarified new understanding of the behaviour of bound excitations and plasmons. Plasmon lifetimes must be finite to agree with causality and experimental data. Plasmon modes are clearly material-specific and so there is no Universal curve; or equivalently that the Universal curve must respond to material-specific excitations. These material-specific plasmon modes must couple, to exchange energy and electron oscillations, and to increase broadening of higher momentum extensions. Solutions should not be arbitrary with infinite Mermin peaks and negative amplitudes. Solutions must also be self-consistent. Excitations below the plasma frequency cutoff are essential to explain observed loss spectra.

Mermin functionals are an essential tool in explaining electron transport properties, obeying sum rules and able to be constant broadening in the optical limit in many-pole models or partial pole representations with increased broadening with q. Recent work is recognising this but there are many additional areas to explore and work on.

The coupled-plasmon model intrinsically accounts for the interaction between different plasmon excitations in the medium, and relaxes the longstanding approximation that a solid is a collection of non-interacting nearly free-electron gases. Our implementation of excitation broadening, which is energy- and momentum-dependent, self-consistent, uniquely constrained, and sensitive to the band structure of the absorbing material, subsequently has a dramatic effect on the electron IMFP.

Refinement with further advanced DFT or other modelling allowing increases to higher energies is a significant but important challenge to current theory. Similarly, inclusion of higher-order effects such as QED self-consistency, correlation, exchange-interference, and excitonic effects may yet contribute significantly, particularly below 100 eV. There is an urgent need for additional high-accuracy measurements of IMFPs, including from XAS, and an associated need for advanced theory to extract the IMFP as close to the edge as possible. Thus far there are far too few experimental datasets. We have concentrated on elements and materials where high quality datasets have been produced; more are in preparation; however, there will be computation of numerous additional reference elements and materials in the near future and the computation of these is well advanced.

The work enables for the first time an approach that includes excitation lifetimes without the need for arbitrary fitting algorithms, meaning that the inclusion of broadening parameters can become standard practice for IMFP determinations. This represents a significant step forward in the understanding of electron transport in general condensed matter systems, and is directly and immediately applicable to all current low-energy electron spectroscopies and microscopies.

Current standard XAFS is a true bulk technique - only bulk plasmons are measured or observed. However, related techniques of 'Normal Incidence' and 'Grazing Incidence' XAFS are intermediate; and ReflEXAFS is almost purely surface plasmonic. Hence while much of this discussion has focussed on bulk plasmons and bulk electronic properties, there are techniques related more directly to surface property measurement to be investigated in the future.

Acknowledgements

The authors acknowledge the work of Z. Barnea, M. D. de Jonge, N. A. Rae and J. L. Glover, and their helpful contribution to the development of ideas important to this research. We also acknowledge the ANBF and AS and staff and access programs for the experimental support of this work.

References

[1] P. Drude, On the electron theory of metals, Ann. Phys. 1 (1900) 566–613.
[2] A. Einstein, The planck theory of radiation and the theory of specific heat, Ann. Phys. 22 (1906) 180–190.
[3] P. Debye, The theory of specific warmth, Ann. Phys. 39 (1912) 789–839.
[4] A. Sommerfeld, On the electron theory of metals due to fermi statistics, Z. Angew. Phys. 47 (1928) 1–32.
[5] A.H. Compton, The spectrum of scattered x-rays, Phys. Rev. 22 (1923) 409–413.
[6] O. Klein, Y. Nishina, About the scattering of radiation by free electrons after the new relativistic quantum dynamics of dirac, Z. Phys. 52 (1929) 853–868.
[7] J. Lindhard, On the properties of a gas of charged particles, Dan. Mat. Fys. Medd. 28 (1954) 1–57.
[8] N.D. Mermin, Lindhard dielectric function in the relaxation-time approximation, Phys. Rev. B 1 (1970) 2362.
[9] C.J. Powell, J.B. Swan, Origin of the characteristic electron energy losses in aluminum, Phys. Rev. 115 (1959) 869–875.
[10] J.D. Jackson, Classical Electrodynamics, second ed., Wiley, NY, 1975.
[11] N.W. Ashcroft, N.D. Mermin, Solid State Physics, Holt, Rinehart, Winston, 1976.
[12] V.B. Berestetskii, E.M. Lifshitz, L.P. Pitaevskii, Quantum Electrodynamics, second ed., Pergamon, 1982.
[13] Z.H. Levine, S.G. Louie, New model dielectric function and exchange-correlation potential for semiconductors and insulators, Phys. Rev. B25 (1982) 6310–6316.
[14] D.R. Penn, Electron mean-free-path calculations using a model dielectric function, Phys. Rev. B 35 (1987) 482–486.
[15] C.T. Chantler, J.D. Bourke, X-ray spectroscopic measurement of photoelectron inelastic mean free paths in molybdenum, J. Phys. Chem. Lett. 1 (2010) 2422.
[16] J.D. Bourke, C.T. Chantler, Measurements of electron inelastic mean free paths in materials, Phys. Rev. Lett. 104 (2010) 206601–206604.
[17] J.D. Bourke, C.T. Chantler, Electron energy loss spectra and overestimation of inelastic mean free paths in many-pole models, J. Phys. Chem. A 116 (2012) 3202.
[18] C.T. Chantler, J.D. Bourke, Electron inelastic mean free path theory and density functional theory resolving discrepancies for low-energy electrons in copper, J. Phys. Chem. A 118 (2014) 909–914.
[19] J.D. Bourke, C.T. Chantler, Momentum-dependent lifetime broadening of electron energy loss spectra: a self-consistent coupled-plasmon model, J Phys. Chem. Letts 6 (2015) 314–319.
[20] W.S.M. Werner, K. Glantschnig, C. Ambrosch-Draxl, Optical constants and inelastic electron-scattering data for 17 elemental metals, J. Phys. Chem. Ref. Data 38 (2009) 1013.
[21] B.I. Lundqvist, Single-particle spectrum of degenerate electron gas 0.2. numerical results for electrons coupled to plasmons, Physik der Kondensiterten Materie 6 (1967) 206.
[22] L. Hedin, B. Lundqvist, S. Lundqvist, New structure in single-particle spectrum of an electron gas, Solid State Commun. 5 (1967) 237.
[23] L. Spruch, Pedagogic notes on thomas-fermi theory (and on some improvements) - atoms, stars, and the stability of bulk matter, Rev. Mod. Phys. 63 (1991) 151–209.
[24] A.P. Sorini, J.J. Kas, J.J. Rehr, M.P. Prange, Z.H. Levine, Ab initio calculations of electron inelastic mean free paths and stopping powers, Phys. Rev. B 74 (2006) 165111–165118.
[25] S. Tanuma, C.J. Powell, D.R. Penn, Calculations of electron inelastic mean free paths. ix. Data for 41 elemental solids over the 50 ev to 30 kev range, Surf. Interface

Anal. 43 (2011) 689.
[26] R.H. Ritchie, A. Howie, Electron excitation and the optical potential in electron microscopy, Philos. Mag. 36 (1977) 463.
[27] C.T. Chantler, J.D. Bourke, Behaviour of low momentum electronic excitations in condensed matter: fundamental consequences from classical and quantum dielectric theory, J. Phys. Condens. Matter 27 (455901) (2015) 1–7.
[28] H. Nikjoo, S. Uehara, D. Emfietzoglou, Interaction of Radiation with Matter, (CRC Press), 2012.
[29] H.-J. Hagemann, W. Gudat, C. Kunz, Deutsches elektronensynchrontron report sr-74/7, DESY Internal Report. Not published. (1974) 1.
[30] E.D. Palik, Handbook of Optical Constants of Solids III, Academic Press: New York, 1998.
[31] W.S.M. Werner, Obtaining quantitative information on surface excitations from reflection electron energy-loss spectroscopy (reels), Surf. Interface Anal. 35 (2003) 347–353.
[32] W.S.M. Werner, Optical constants of cu measured with reflection electron energy loss spectroscopy (REELS), Surf. Sci. Lett. 600 (2006) L250–L254.
[33] W.S.M. Werner, Analysis of reflection electron energy loss spectra (REELS) for determination of the dielectric function of solids: Fe, co, ni, Surf. Sci. 601 (2007) 2125–2138.
[34] W.S.M. Werner, Simple algorithm for quantitative analysis of reflection electron energy loss spectra (REELS), Surf. Sci. 604 (2010) 290–299.
[35] D. Tahir, S. Tougaard, Electronic and optical properties of Cu, CuO and Cu2O studied by electron spectroscopy, J. Phys. 24 (2012) 175002.
[36] M. Vos, Extracting detailed information from reflection electron energy loss spectra, J. Elec. Spectrosc. Rel. Phenom. 191 (2013) 65.
[37] C.J. Tung, J.C. Ashley, R.H. Ritchie, Electron inelastic mean free paths and energy losses in solids ii, Surf. Sci. 81 (1979) 427–439.
[38] D.Y. Smith, E. Shiles, Finite-energy f-sum rules for valence electrons, Phys. Rev. B 17 (1978) 4689.
[39] C.D. Denton, I. Abril, R. Garcia-Molina, J.C. Moreno-Marin, S. Heredia-Avalos, Influence of the description of the target energy-loss function on the energy loss of swift projectiles, Surf. Inter. Anal. 40 (2008) 1481–1487.
[40] B. Da, H. Shinotsuka, H. Yoshikawa, Z.J. Ding, S. Tanuma, Extended mermin method for calculating the electron inelastic mean free path, Phys. Rev. Lett. 113 (2014) 063201.
[41] C.T. Chantler, J.D. Bourke, Full-potential theoretical investigations of electron inelastic mean free paths and extended x-ray absorption fine structure in molybdenum, J. Phys. 26 (145401) (2014) 1–8.
[42] C.M. Kwei, Y.F. Chen, C.J. Tung, J.P. Wang, Electron inelastic mean free paths for plasmon excitations and interband transitions, Surf. Sci. 293 (1993) 202–210.
[43] W.S.M. Werner, C. Tomastik, T. Cabela, G. Richter, H. Stori, Elastic electron reflection for determination of the inelastic mean free path of medium energy electrons in 24 elemental solids for energies between 50 and 3400 ev, J. Electron. Spectrosc. 199 (2001) 127–135.
[44] G. Gergely, Elastic backscattering of electrons: determination of physical parameters of electron transport processes by elastic peak electron spectroscopy, Prog. Surf. Sci. 71 (2002) 31–88.
[45] A. Jablonski, C.J. Powell, Effective attenuation lengths for photoelectrons emitted by high-energy laboratory x-ray sources, J. Electron. Spectrosc. 199 (2015) 27–37.
[46] C.T. Chantler, Z. Barnea, C.Q. Tran, J.B. Tiller, D. Paterson, Precision x-ray optics for fundamental interactions in atomic physics, resolving discrepancies in the x-ray regime, Opt. Quantum Electron. 31 (5–7) (1999) 495–505.
[47] C.T. Chantler, C.Q. Tran, Z. Barnea, D. Paterson, D.J. Cookson, D.X. Balaic, Measurement of the x-ray mass attenuation coefficient of copper using 8.85–20 keV synchrotron radiation, Phys. Rev. A 64 (2001) 062506,1–15.
[48] J.L. Glover, C.T. Chantler, The analysis of x-ray absorption fine structure: beam-line independent interpretation, Meas. Sci. Technol. 18 (2007) 2916–2920.
[49] J.L. Glover, C.T. Chantler, Z. Barnea, N.A. Rae, C.Q. Tran, Measurement of the x-ray mass-attenuation coefficients of gold, derived quantities between 14 kev and 21 kev and determination of the bond lengths of gold, J. Phys. B 43 (2010) 085001(1–15).
[50] C.T. Chantler, Development and applications of accurate measurement of x-ray absorption: the x-ray extended range technique for high accuracy absolute xafs by transmission and fluorescence, Eur. Phys. J. 169 (2009) 147–153.
[51] C.T. Chantler, Accurate measurement and physical insight: the X-ray extended range technique for fundamental atomic physics, condensed matter research and biological sciences, Radiat. Phys. Chem. 79 (2) (2010) 117–123.
[52] M.T. Islam, C.T. Chantler, L.J. Tantau, C.Q. Tran, M.H. Cheah, A.T. Payne, S.P. Best, Structural investigation of mM Ni (II) complex isomers using transmission XAFS: the significance of model development, J. Synchrotron Radiat. 22 (2015) 1475–1491.
[53] J.D. Bourke, C.T. Chantler, Y. Joly, FDMX: extended x-ray absorption fine structure calculations using the finite difference method, J. Synchrotron Radiat. 23 (2016) 551–559.
[54] E.C. Cosgriff, C.T. Chantler, C. Witte, L.F. Smale, C.Q. Tran, Atomic cluster-structure calculations of the x-ray near-edge absorption of silver, Phys. Lett. A 343 (2005) 174–180.
[55] C. Witte, C. Chantler, E.C. Cosgriff, C.Q. Tran, Atomic cluster calculation of the x-ray near-edge absorption of copper, Radiat. Phys. Chem. 75 (2006) 1582–1585.
[56] J. Bourke, C. Chantler, C. Witte, Finite difference method calculations of x-ray absorption fine structure for copper, Phys. Lett. A 360 (6) (2007) 702–706.
[57] J.D. Bourke, C.T. Chantler, Finite difference method calculations of long-range x-ray absorption fine structure for copper over k 20a-1, Nucl. Instr. Meth. A 619 (2010) 33–36.
[58] J.D. Bourke, M.T. Islam, S.P. Best, C.Q. Tran, F. Wang, C.T. Chantler, Conformation analysis of ferrocene and decamethylferrocene via full-potential modeling of XANES and XAFS spectra, J. Phys. Chem. Lett. 7 (14) (2016) 2792–2796.
[59] C.T. Chantler, C.Q. Tran, Z. Barnea, D. Paterson, D. Cookson, D.X. Balaic, Measurement of the x-ray mass attenuation coefficient of copper using 8.85 20 kev synchrotron radiation, Phys. Rev. A 64 (2001) 062506.
[60] Z.-J. Ding, R. Shimizu, Inelastic collisions of kv electrons in solids, Surf. Sci. 222 (1989) 313–331.
[61] S. Tanuma, C.J. Powell, D.R. Penn, Calculations of electron inelastic mean free paths. ii. data for 27 elements over the 50–2000 ev range, Surf. Interface Anal. 17 (1991) 911–926.
[62] J.C. Ashley, Energy loss rate and inelastic mean free path of low-energy electrons and positrons in condensed matter, J. Electron Spectrosc. Relat. Phenom. 50 (1990) 323.
[63] J.L. Glover, C.T. Chantler, Z. Barnea, N.A. Rae, C.Q. Tran, D.C. Creagh, D. Paterson, B.B. Dhal, Measurements of the x-ray mass-attenuation coefficient and imaginary component of the form factor of copper, Phys. Rev. A 78 (2008) 052902.
[64] D. Emfietzoglou, F.A. Cucinotta, H. Nikjoo, A complete dielectric response model for liquid water: a solution of the bethe ridge problem, Radiat. Res. 164 (2005) 202.
[65] C.T. Chantler, J.D. Bourke, Investigation of momentum-dependent lifetime broadening of electron energy loss spectra: sum rule constraints and an asymmetric rectangle toy model, Phys. Rev. B 90 (174306) (2014) 1–8.
[66] J.D. Bourke, C.T. Chantler, Low-energy electron energy losses and inelastic mean free paths in zinc, selenium, and zinc selenide, J. Elec. Spec. Rel. Phenom. 196 (2014) 142–145.
[67] H.T. Nguyen-Truong, Energy-loss function including damping and prediction of plasmon lifetime, J. Electron Spectrosc. Relat. Phenom. 193 (2014) 79–85.
[68] H.T. Nguyen-Truong, Penn algorithm including damping for calculating the electron inelastic mean free path, J Phys. Chem. C 119 (2015) 7883–7887.
[69] H.T. Nguyen-Truong, Low energy electron inelastic mean free path in materials, App. Phys. Lett. 108 (2016) 172901.
[70] H.T. Nguyen-Truong, Electron inelastic mean free path at energies below 100 ev, J Phys. Condens. Matter 29 (2017) 215501.
[71] P. de Vera, R. Garcia-Molina, Electron inelastic mean free paths in condensed matter down to a few electronvolts, arXiv.1807.11710v1 31/7/2019 (2018) 1.
[72] M. Vos, P.L. Grande, The relation between the electron energy loss spectra of hafnia and its dielectric function, Surf. Sci. 630 (2014) 1–8.
[73] M. Vos, A model dielectric function for low and very high momentum transfer, NIM B 366 (2016) 6–12.
[74] M. Vos, P.L. Grande, Simple model dielectric functions for insulators, J. Phys. Chem. Solids 104 (2017) 192–197.
[75] M. Vos, P.L. Grande, Extracting the dielectric function from high-energy reels measurements, Surf. Interface Anal. 49 (2017) 809–821.
[76] E.L. Shirley, Ab initio inclusion of electron-hole attraction: application to x-ray absorption and resonant inelastic x-ray scattering, Phys. Rev. Lett. 80 (1998) 794–797.
[77] J. Vinson, J.J. Rehr, J.J. Kas, E.L. Shirley, Bethe-salpeter equation calculations of core excitation spectra, Phys. Rev. B 83 (2011) 115106.